Analysis of the Radiation Field Generated by 200-MeV Electrons on a Target at the CLEAR Accelerator at CERN

Giuseppe Lerner, Pierre Pelissou, Ygor Q. Aguiar, *Member, IEEE*, Mario Sacristan Barbero, *Member, IEEE*, Matteo Cecchetto, Kacper Biłko, Louise Coussen, Natalia Emriskova, Rubén García Alía, *Member, IEEE*, Luke Dyks, and Wilfrid Farabolini

***Abstract*— The radiation showers generated by the interaction of high-energy electrons with matter include neutrons with an energy distribution peaked at the MeV scale, produced via photonuclear reactions, allowing measurements of neutron-induced single-event effects (SEEs) in electronic devices. In this work, we study a setup where the 200-MeV electron beam of the CLEAR accelerator at European Organization for Nuclear Research [Centre Européen pour la Recherche Nucléaire (CERN)] is directed on an aluminum target to produce a radiation field with a large neutron component. The resulting environment is analyzed by measuring the single-event upset (SEU) and latchup rates in well-characterized static random access memories (SRAMs), as well as the total ionizing dose (TID) in passive radio-photoluminescence (RPL) dosimeters, and by comparing the results with predictions from FLUKA simulations. We find that a lateral shielding made of lead protects the SRAMs from an excessive TID rate, yielding an optimal configuration for SEU measurements, particularly in SRAMs that are highly sensitive to MeV-scale neutrons. This setup provides an interesting complementary neutron source with respect to standard neutron facilities based on spallation targets or radioactive sources.**

***Index Terms*— Accelerator, European Organization for Nuclear Research [Centre Européen pour la Recherche Nucléaire (CERN)], CERN linear electron accelerator for research (CLEAR), electrons, neutrons, photons, radiation effects to electronics (R2E), single-event effects (SEEs), single-event latchup (SELs), single-event upsets (SEUs), total ionizing dose (TID).**

I. Introduction

THE radiation field produced by the impact of multi-MeV electron beams on target materials is dominated by electromagnetic showers, but if the energy is sufficiently large (generally above a few tens of MeV, with a dependence on the material), it also contains the products of photonuclear reactions, notably neutrons. In the context of radiation effects to electronics (R2E), the European Organization for Nuclear Research [Centre Européen pour la Recherche Nucléaire (CERN)] linear electron accelerator for research (CLEAR) [1] has been exploited in the past for in-beam irradiations, measuring electron-induced effects in memories [2], [3], [4], and recently also for off-beam radiation field analyses focusing on the measurement of the neutron flux [5]. The latter study demonstrated that the flux of neutrons produced in the CLEAR beam dump is sufficient to induce single-event upsets (SEUs) in static random access memories (SRAMs) [6]. Following these findings, we now present an experimental setup where the electron beam is directed on a cylindrical target made of an aluminum alloy (6082), optimized to obtain test positions where the neutron flux is strongly enhanced compared with the one that was measured in [5]. This document describes the results of a test campaign involving total ionizing dose (TID) measurements with radio-photoluminescence (RPL) dosimeters [7], [8] and SEU and single-event latchup (SEL) measurements with different SRAMs [9], [10], [11], analyzing the properties of the proposed setup and confirming that it is promising for applications in the radiation effects field and beyond.

Manuscript received 10 January 2023; revised 9 February 2023; accepted 19 February 2023. Date of publication 10 March 2023; date of current version 16 August 2023.

Giuseppe Lerner, Ygor Q. Aguiar, Mario Sacristan Barbero, Matteo Cecchetto, Kacper Biłko, Natalia Emriskova, and Rubén García Alía are with CERN, CH-1211 Geneva, Switzerland.

Pierre Pelissou and Louise Coussen are with CERN, CH-1211 Geneva, Switzerland, and also with INSA Toulouse, 31400 Toulouse, France.

Luke Dyks is with CERN, CH-1211 Geneva, Switzerland, and also with the Department of Physics, University of Oxford, OX1 2JD Oxford, U.K.

Wilfrid Farabolini is with CERN, CH-1211 Geneva, Switzerland, and also with CEA-Saclay, 91191 Gif-sur-Yvette, France.

Color versions of one or more figures in this article are available at https://doi.org/10.1109/TNS.2023.3252808.

Digital Object Identifier 10.1109/TNS.2023.3252808

II. Radiation Field Properties

A. Electromagnetic Shower and Photonuclear Reactions

The impact of an electron beam with energy on the order of 200 MeV on a target produces radiation showers driven by the following processes taking place in the target core:

1) development of an electromagnetic cascade with photons emitted via bremsstrahlung and electron–positron pairs;
2) production of neutrons via photonuclear reactions initiated by photons and, with minor probability, via electronuclear reactions initiated by electrons [12].

As a result of these processes, in the vicinity of the target, a mixed radiation field is generated, including almost exclusively electromagnetic particles (electrons, positrons, and photons) and, importantly, neutrons. A thorough characterization of this field, with particular focus on the neutrons, is essential to determine the suitability of the proposed setup for applications in the context of R2E.

B. Radiation Field Simulations and Measurements for R2E

During the design and analysis phases of the experimental tests presented in this article, the Monte Carlo code

FLUKA [13], [14], [15] was employed to simulate the radiation showers in geometry models replicating the experimental setups, describing the radiation field properties and deriving predictions for comparison with the experimental results. As anticipated, the latter consists of SEU and SEL rate measurements in well-characterized SRAMs used as radiation monitors, and in TID rates measured with passive RPL dosimeters.

Concerning single-event effects (SEEs), the analysis strategy relies on the well-justified assumption that the rates measured by the SRAMs in the test positions (further described in Section III) are exclusively driven by neutrons, as supported by previous studies and observations (e.g., in [2] and [5]) combined with FLUKA-based analyses of neutron and electromagnetic particle fluxes. Under this assumption, when using SRAMs with well-known neutron response, the neutron energy spectra simulated with FLUKA can indeed be used to obtain SEE rate predictions to be compared with the measurements, yielding the desired experimental validation of the simulated field properties.

To do so, we rely on a set of commercial SRAMs that were characterized in previous experimental campaigns under the high energy hadron (HEH) approximation [9], [16]. In its simplest version, this approximation consists in expressing the SEE rate as the product of a device-specific cross section ($\sigma_{\text{sat}}^{\text{HEH}}$) and the HEH flux, defined as the flux of hadrons with $E > 20$ MeV. In other words, this corresponds to assuming that hadrons have a step-like SEE cross section as a function of energy, null below the 20 MeV threshold and constant above it. The HEH approximation is commonly applied to all hadrons that induce SEEs via indirect ionization, but for the purpose of this article, we can focus exclusively on the neutrons, as any other hadron type is essentially absent from the radiation field.

As discussed in detail in [17] and in the references therein, when measuring SELs, the basic version of the HEH flux is commonly used, because the SEL cross section of neutrons below 20 MeV is typically negligible. Instead, in the case of SEUs, electronic devices can also be sensitive to neutrons with energy ranging from a fraction of MeV to the 20-MeV threshold (the so-called intermediate-energy range). While other options are possible, a common parametrization of the cross section of neutron-induced SEUs in the intermediate-energy range is the emphirical Weibull function

$$\sigma(E) = \sigma_{\text{sat}}^{\text{HEH}}\left[1 - e^{-((E-E_0)/W)^S}\right] \tag{1}$$

where E is the neutron energy, E_0 is the lower energy threshold (typically a fraction of MeV), W is the scale parameter (in energy units), S is the dimentionless shape parameter, and $\sigma_{\text{sat}}^{\text{HEH}}$ is the saturation cross section introduced above. To account for the non-negligible SEU response to intermediate-energy neutrons, the radiation field can be quantified by defining a more complex HEH equivalent flux (HEH-eq) given by the sum of the HEH flux and the flux of intermediate-energy neutrons weighted by the Weibull parameters [i.e., the bracket part in (1)]. Notably, due to these parameters, the value of the HEH-eq flux for a given radiation field is device-dependent.

TABLE I

SATURATION CROSS SECTION AND WEIBULL PARAMETERS OF ISSI (DATE CODE 1650, REF. IS61WV204816BLL-10TLI), CYPRESS-65 nm (CY65, DATE CODE 1731, REF. CY62167GE30-45ZXI), AND CYPRESS-90 nm (CY90, DATE CODE 1843, REF. CY62157EV30LL-45ZSXI) SRAMS FOR SEU MEASUREMENTS [18]

	N_{bit}	$\sigma_{\text{sat}}^{\text{HEH}}$ [cm^2/bit]	E_{th} [MeV]	W [MeV]	S
ISSI	32 M	$1.40 \cdot 10^{-14}$	0.01	14.05	0.82
Cy65	16 M	$7.73 \cdot 10^{-14}$	0.01	11.57	0.80
Cy90	8 M	$2.16 \cdot 10^{-13}$	0.1	24.22	1.98

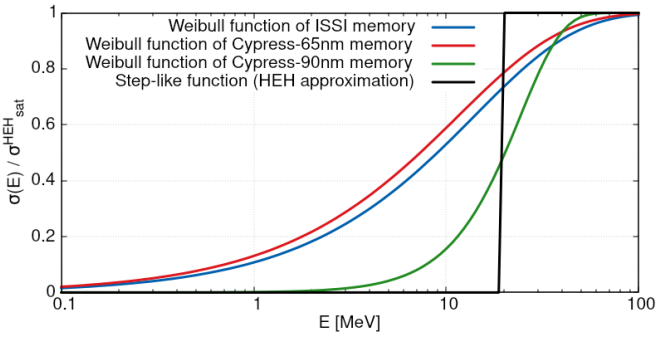

Fig. 1. Weibull functions of the SRAMs used in the test, obtained through (1) with the parameters in Table I, compared with the step-like response of the SEE cross section under the HEH approximation.

TABLE II

SRAM MEMORIES USED TO MEASURE SELS [9], [10]

	N_{bit}	$\sigma_{200\ \text{MeV}}^{\text{HEH}}$ [cm^2/chip]	Reference
Lyontek	16 M	$4.6 \cdot 10^{-8}$	LY62W20488ML-55LL
ISSI	4 M	$2.3 \cdot 10^{-8}$	IS61LV5128AL-10TLI
Samsung	4 M	$4.4 \cdot 10^{-10}$	K6R4016V1D-TC10
Alliance	4 M	$3.4 \cdot 10^{-10}$	AS7C34098A-10TCN

The saturation cross sections and the Weibull parameters of the commercial SRAMs used in the test (ISSI, Cypress-65 nm, and Cypress-90 nm [18]) are reported in Table I, and the resulting $\sigma(E)/\sigma_{\text{sat}}^{\text{HEH}}$ curves are displayed in Fig. 1 along with the step-like response used in the basic HEH approximation. From the figure, it is clear that Cypress-90 nm is less sensitive to intermediate-energy neutrons compared with the other SRAMs measuring SEUs. For completeness, we also report in Table II the SRAMs used to measure the SEL rate (Lyontek, ISSI, Samsung, and Alliance [9], [10]) with the associated cross sections measured with 200-MeV protons.

By parametrizing the SEE response via the Weibull parameters, the FLUKA Monte Carlo code can be used to compute the device-dependent HEH-eq flux for all the SRAMs. The expected SEE rate is then simply obtained as the product of the HEH-eq flux and the corresponding $\sigma_{\text{sat}}^{\text{HEH}}$ from Table I, further scaled with the number of bits of the SRAM, and ready to be directly compared with the experimental results. The calculation of the expected rate is also done for the SELs, using the simple HEH flux and the cross sections in Table II.

A priori, an additional contribution to the SEU rate could come from thermal-energy neutrons [19]. With regard to these,

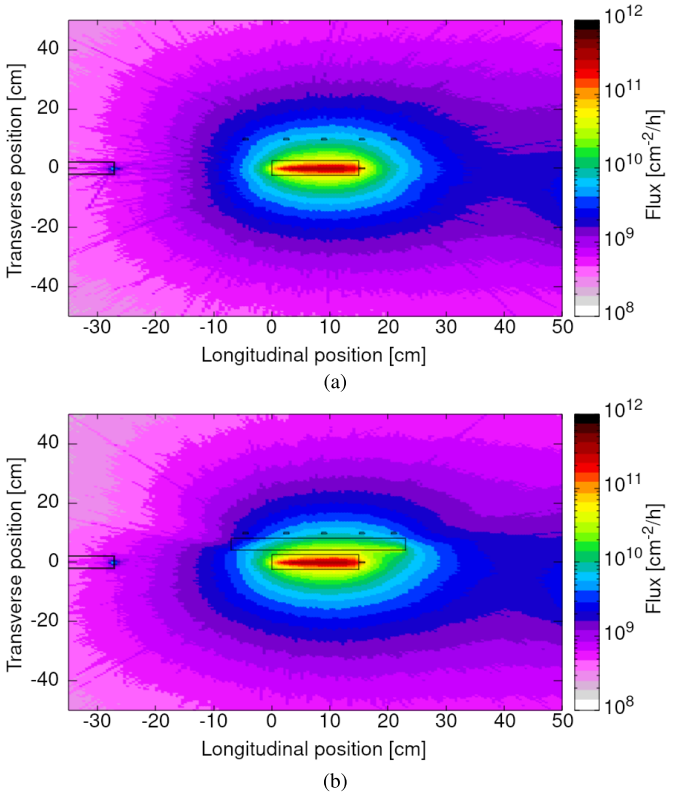

Fig. 2. FLUKA simulation of the ISSI HEH-eq flux around the target for high-intensity CLEAR operation in (a) Run 2 and (b) Run 3, i.e., in the absence and presence of lateral Pb shielding (see Section III). The electron beam is coming from the left-hand side of the figure, and it hits the target at $z = 0$ cm.

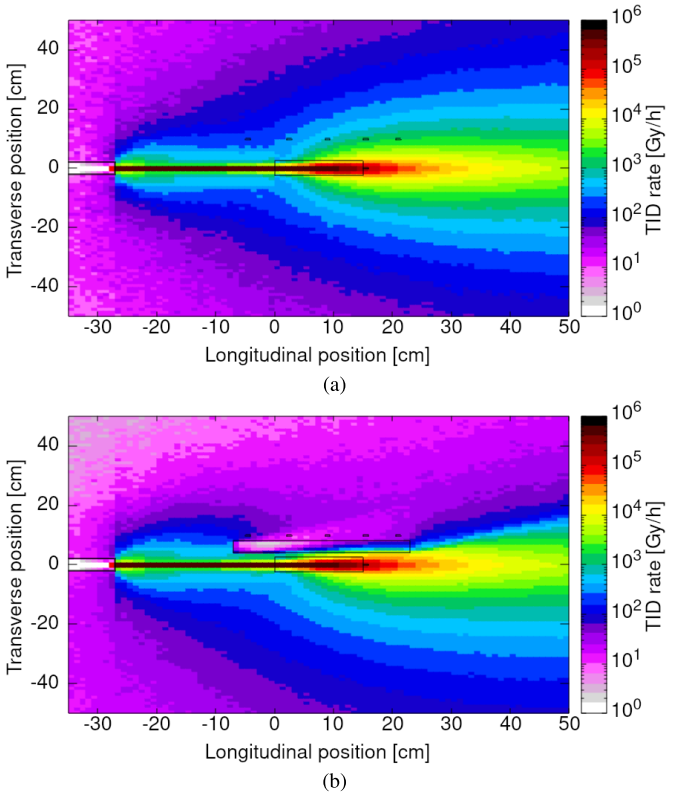

Fig. 3. FLUKA simulation of the TID rate around the target for high-intensity CLEAR operation in (a) Run 2 and (b) Run 3, i.e., in the absence and presence of lateral Pb shielding (see Section III). The electron beam is coming from the left-hand side of the figure, and it hits the target at $z = 0$ cm.

FLUKA studies show that the neutron thermalization process is almost exclusively driven by the materials surrounding the setup (e.g., the concrete walls of the facility) and not by the target itself. In addition, as further shown in Section II-C, the thermal neutron flux at the positions of interest near the target is negligible compared with the flux of higher-energy neutrons, so in this document, we neglect the associated contribution to the SEU rates.

Concerning cumulative effects, the FLUKA code is used to compute the TID deposited in RPL dosimeters, generally dominated by electromagnetic particles. In addition, it can predict the silicon 1-MeV neutron equivalent flux (1MeVn-eq) quantifying displacement damage (DD) effects [20].

C. Radiation Field Maps Near the Target

Figs. 2 and 3 show a map of the ISSI HEH-eq flux and the TID rate simulated with FLUKA for a 205-MeV electron beam with negligible width impacting on an Al-alloy (6082) target with a radius of 2.5 cm and a length of 15 cm. While both radiation fields present a cylindrical symmetry, as expected due to the geometry of the setup, the two maps are exhibiting important differences: the TID has a conical shape with peak values downstream of the target close to the beam axis, whereas the HEH-eq flux is distributed more uniformly. In fact, the different shapes of the radiation maps are reflecting their respective origins: while the TID is mostly deposited by electrons, positrons, and photons from electromagnetic showers, that are dominant downstream of the target, the HEH-eq flux consists of neutrons from photonuclear reactions, that retain relatively larger fluxes in transverse positions.

Each plot in Figs. 2 and 3 is presented for two configurations of the setup, with and without a 5-cm-thick Pb shielding on one side of the target. The shielding yields a visible reduction of both the HEH-eq flux and the TID rate, but the reduction of the TID rate is clearly more significant. This observation indicates that a lateral shielding element can be used to enhance the ratio between HEH-eq flux and TID rate, resulting in optimal radiation field conditions for SEE measurements.

Fig. 4 presents the top views of the HEH flux (without intermediate-energy neutron contribution) and the 1MeVn-eq flux, which quantifies the DD to materials, focusing only on the configuration without lateral Pb shielding. The shape of the HEH flux map around the target is similar to the HEH-eq flux, as expected. However, the HEH flux is significantly lower in absolute value, due to the low proportion of neutrons with energy above 20 MeV in the radiation field, as further described below. Instead, the 1MeVn-eq flux has a shape that resembles more the one of the TID rate: while this may seem counter-intuitive, it can be explained by considering that electrons are also contributing to the 1MeVn-eq flux, and that the electron flux downstream of the target is substantially higher compared with the flux of neutrons.

The energy spectrum of neutrons on the side of the target is shown in Fig. 5 as a lethargy plot (i.e., showing the

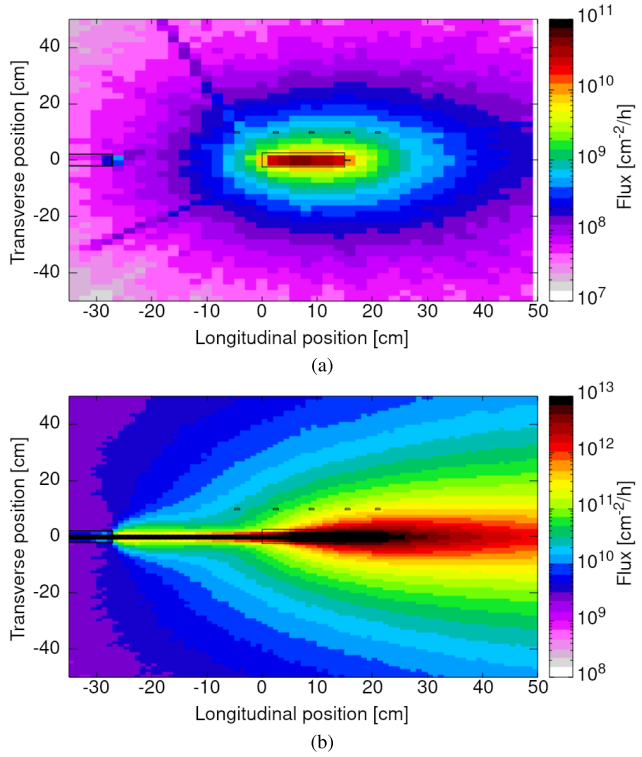

Fig. 4. FLUKA simulation of (a) HEH flux and (b) 1MeVn-eq flux near the target for high-intensity CLEAR operation. The electron beam is coming from the left-hand side of the figure, and it hits the target at $z = 0$ cm. This simulation is representative of Run 2 of the test campaign (see Section III).

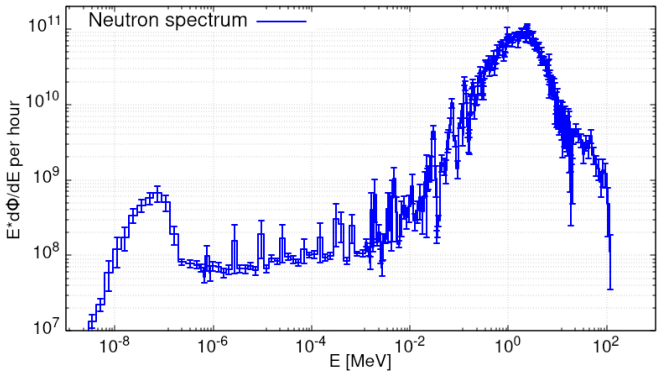

Fig. 5. FLUKA simulation of neutron lethargy spectrum on the target side.

differential neutron flux per unit logarithm of the energy, with both axes in logarithmic scale). The spectrum extends up to more than 100 MeV but peaking around 1 MeV, i.e., precisely in the intermediate-energy range of neutrons where the SEU cross section is strongly dependent on the specific devices, as illustrated by the Weibull curves of the different SRAMs in Fig. 1. The thermal neutron peak is driven by the presence of concrete in the experimental area surrounding the test setup, but its size is much smaller, so it is safe to neglect the associated contribution to the SEE rates.

III. CLEAR Test Campaign

A. Experimental Setup

The FLUKA maps in Figs. 2–4 indicate that, in the off-axis positions near the target, the HEH-eq flux can be maximized while retaining a relatively low TID, especially when using extra lateral shielding. As anticipated in Section II-B, based on the experience gained in [2] and [5], in such positions, it is safe to expect that the rate of SEEs measured by SRAMs is entirely dominated by the HEH-eq flux, while the effect of electrons, positrons, and photons is limited to the associated TID deposition. Incidentally, this assumption may not hold in positions where the flux of multi-MeV electromagnetic particles is significantly larger than the neutron flux, e.g., downstream of the target, where the ratio between TID and HEH-eq flux is also much higher. For a discussion of SEUs induced by electromagnetic particles, the reader can refer to [2].

The above considerations are clearly indicating that transverse positions with respect to the target present the best properties to perform SEE measurements. For this reason, we prepared the test setup shown in Fig. 6, where the electron beam of CLEAR impacts a 15-cm-long target, as in the simulations shown above. Four SRAMs (two ISSI, one Cypress-65 nm, and one Cypress-90 nm, as described in Table I) are disposed on two panels both placed at 10 cm from the beam axis (a lateral panel and a top panel), such that, owing to the cylindrical symmetry of the setup, they are exposed to an equivalent radiation field. The SRAMs are placed on the test boards with their standard package, which has a negligible effect on the incoming neutron flux. The panels are also hosting two arrays of five RPL dosimeters each, measuring the TID as a function of the longitudinal position parallel to the target. Finally, one more RPL has been used to measure the TID downstream of the target on the beam axis.

A similar setup was used to measure SELs, using the SRAMs listed in Table II, once again in their standard package. In this case, the SRAMs were arranged in pairs on the lateral panel only, that could host two of them at a time.

In summary, four configurations of the setup (all individually simulated with FLUKA) were used to measure the rate of TID, SEUs, and SELs with a variable amount of material between the beam axis and the radiation monitors.

1) *RUN 1 (SEU and TID Measurements on Lateral and Top Panels):* 15-cm-long target with 5-cm radius.
2) *RUN 2 (SEU and TID Measurements on Lateral and Top Panels):* 15-cm-long target with 2.5-cm radius.
3) *RUN 3 (SEU and TID Measurements on Lateral and Top Panels):* 15-cm-long target with 2.5-cm radius, with 5-cm-thick Pb shielding between the target and the lateral panel.
4) *RUN 4 (SEL Measurements on Lateral Panel, With Two SRAMs at a Time):* 30-cm-long target with 5-cm radius, with 10-cm-thick Pb and Fe shielding between the target and the lateral panel.

B. CLEAR Beam Parameters

During the test, the CLEAR accelerator operated with sequences of electron bunches on the target (referred to as trains) at a rate of 10 Hz (more details in [21]). While the time structure of the beam can play a role when performing specific tests, this was not the case for the SEE measurements

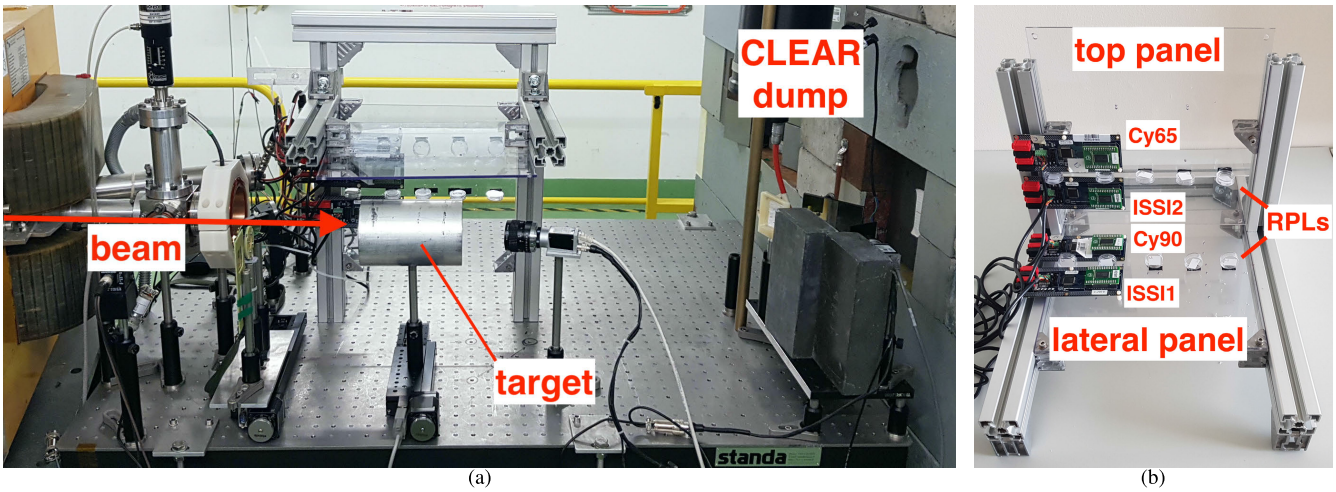

(a) (b)

Fig. 6. Full view of (a) test setup at CLEAR and (b) detail of the support structure hosting the two panels with RPLs and SRAMs in Run 1, Run 2, and Run 3. The same support structure is used in Run 4, hosting different SRAMs to measure SELs.

presented in this study, as the impact of electromagnetic particles is negligible (as argued above), and the neutron flux is too low for any pileup effect to occur during the arrival of single bunches or trains. Similarly, no effect linked to a high TID rate is expected in the positions of interest. For each setup in our test campaign, the radiation level quantities (e.g., particle fluxes, the TID, and the SRAM SEE rates) are, hence, simply proportional to the cumulative beam intensity on the target. To facilitate the comparison between experimental runs during which the beam intensity was not always identical for practical reasons, we present normalized results by scaling the measured and simulated radiation levels to 1 h of high-intensity CLEAR operation with a train charge of 30 nC, corresponding to $6.75 \cdot 10^{15}$ electrons on target per hour.

In terms of beam energies, the electrons were accelerated up to approximately 205 MeV during Run 1, Run 2, and Run 3. During Run 4, which was divided into two parts (testing first the ISSI and Lyontek SRAMs, and then the Samsung and Alliance ones), the beam energy was measured to be a bit lower, and with a wider distribution extending over a few tens of MeVs (see the next paragraph for further details). The different energy of the electrons has been taken into account in the respective FLUKA simulations: while its impact on the radiation field rates is not entirely negligible, it does not substantially alter the general properties of the setup.

IV. Test Results

A. TID Measurements and FLUKA Predictions

As anticipated, during Run 1, Run 2, and Run 3, the RPL dosimeters have been arranged in two arrays parallel to the beam axis on the two panels, while one extra RPL has been placed downstream of the target (only during Run 2 and Run 3). The results of the TID measurements of the latter RPLs are presented in Table III with the corresponding FLUKA predictions expressed as hourly TID rate for the reference CLEAR intensity described in Section III-B, showing that a remarkable TID rate of around 300 kGy/h is reached.

TABLE III
TID Rate Measured by RPL Dosimeters Downstream of the Target in Run 2 and Run 3 Scaled to High-Intensity CLEAR Operation, Compared With FLUKA Simulations

	Simulated TID rate [Gy / h]	Measured TID rate [Gy / h]
Run 2	$(2.7 \pm 0.4) \cdot 10^5$	$(2.54 \pm 0.08) \cdot 10^5$
Run 3	$(2.7 \pm 0.2) \cdot 10^5$	$(3.17 \pm 0.10) \cdot 10^5$

The results of the RPL array measurements on the lateral and top panels are presented in Fig. 7, in generally good agreement with the FLUKA predictions. Coherently with the map shown in Fig. 3(a), the TID rate increases as a function of the longitudinal position, with a maximum value on the two panels on the order of 1 kGy/h. Even though it is much lower than that downstream of the target (Table III), this TID rate is still significant for possible effects on commercial components, implying that the more upstream positions with a lower TID rate are to be preferred for SEE measurements. The TID rates in the two panels are consistent between each other during Run 1 and Run 2, with higher rates in Run 2 compared with Run 1 due to the lateral shielding effect provided by the larger target radius in Run 1. In Run 3, the TID rate drops substantially on the lateral panel, due to the important impact of the Pb shielding, whereas the difference between Run 2 and Run 3 results is negligible in the top panel, which is not shielded. In practice, the TID levels on the lateral panel in Run 3 are the lowest, as expected based on the FLUKA simulations, making this the optimal configuration for SEE tests. The agreement between FLUKA predictions and measured data is satisfactory also in these positions, with the partial exception of the first two RPLs where a relatively larger deviation was observed, which we attribute to possible small inaccuracies of the FLUKA geometry model in the upstream part of the Pb shielding. Even with these caveats, the overall picture clearly confirms that the TID map around the target is well modeled by the FLUKA simulation.

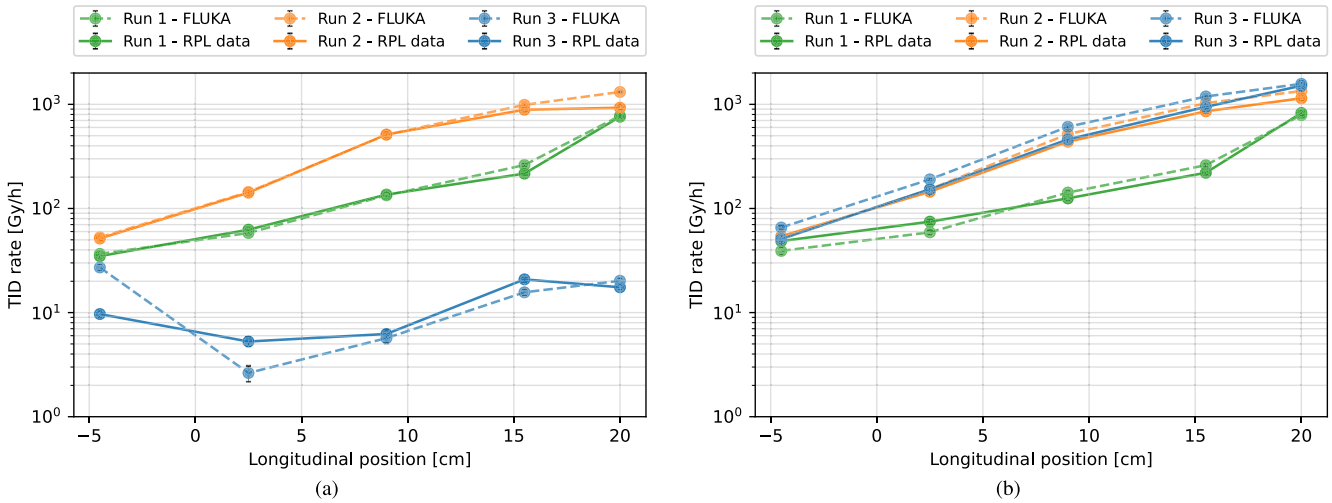

Fig. 7. Measured TID rate per hour in (a) lateral and (b) top panels scaled to high-intensity CLEAR operation, in comparison with FLUKA predictions.

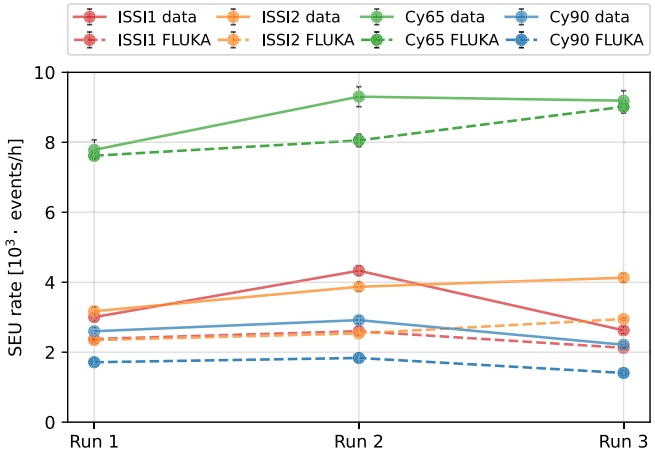

Fig. 8. SRAM SEU rate per hour scaled to high-intensity CLEAR operation, in comparison with FLUKA-based predictions. The error bars include the Poisson statistics and the Monte Carlo uncertainty, respectively.

B. SEU Measurements and FLUKA-Based Predictions

The SRAM SEU rates in Run 1, Run 2, and Run 3 are presented in Fig. 8, scaled to high-intensity CLEAR operation. The data are compared with predictions obtained from the saturation cross sections and the HEH-eq fluxes simulated with FLUKA, computed for each SRAM with the respective Weibull parameters. The measured SEU rates show mild excesses (below 40%) with respect to the predictions, which is a satisfactory level of agreement, as the predictions carry non-negligible uncertainties. Indeed, the measured SRAM SEU cross sections at the MeV scale have been found to differ by similar amounts from the Weibull interpolations (see, e.g., the comparisons in [18]). The observed level of agreement between measurements and predictions for SRAMs with different response to intermediate-energy neutrons can be regarded as a strong confirmation of the validity of the simulated neutron energy spectrum shown in Fig. 5.

The results show that for high-intensity CLEAR operation, all SRAMs reach a rate of more than 10^3 SEUs/h, with the Cypress-65 nm reaching almost 10^4 SEUs/h. Using the Run 1 simulated values as an example, the HEH-eq flux ranged between $9.5 \cdot 10^8$ cm^{-2}/h for the Cypress-90 nm and $5.9 \cdot 10^9$ cm^{-2}/h for the Cypress-65 nm owing to the different Weibull parameters and the neutron spectrum peak at the MeV scale. For this reason (and due to the lower number of bits), the Cypress-90 nm measured the lowest SEU rate despite having a higher saturation cross section compared with the other SRAMs in use.

While the SEU rates are affected by the different target radii (as seen by comparing Run 1 and Run 2) and by the Pb shielding (as seen by comparing Run 3 and Run 2 for the SRAMs on the lateral panel, i.e., ISSI1 and Cypress-65 nm), the associated variations are much smaller compared with the case of the TID rate. Based on this evidence, it is clear that the addition of shielding around the target is a powerful way to suppress the TID rate without spoiling excessively the neutron flux, hence obtaining an optimal configuration for SEE measurements.

C. SEL Measurements and FLUKA-Based Predictions

The results of the SEL measurements carried out during Run 4 are presented in Table IV, again scaled to the high-intensity CLEAR operation with 30 nC per train, which corresponds to $6.75 \cdot 10^{15}$ electrons on target per hour. The table includes the FLUKA prediction of the HEH flux without the intermediate-energy neutron component, following the approach outlined in Section II-B. The measured SEL rate is substantially lower than the SEU rate, and in the case of the Samsung and Alliance SRAMs, no SEL event was measured at all. This observation is fully consistent with the simulated neutron energy spectrum shown in Fig. 5, which manifests itself also in the difference between the HEH-eq fluxes of the different SRAMs (especially the Cypress-65 nm and the ISSI) and the HEH flux that includes only neutrons with energy above 20 MeV.

Finally, Table IV also includes a computation of the SEL cross section of each SRAM, obtained as the ratio between the measured SEL rate and the FLUKA HEH flux, further divided by 8 to obtain the cross section per chip (as each board hosted eight units). The Lyontek and ISSI SEL cross sections

TABLE IV

FLUKA PREDICTIONS AND RESULTS OF THE SEL MEASUREMENTS CARRIED OUT DURING RUN 4. THE HEH FLUX IS COMPUTED WITH FLUKA, WITHOUT THE CONTRIBUTION OF INTERMEDIATE-ENERGY NEUTRONS, WHILE THE MEASURED SEL RATE IS REPORTED IN THE TABLE AFTER SCALING IT TO 1 H OF OPERATION AT 30 nC PER TRAIN ($6.75 \cdot 10^{15}$ ELECTRONS ON TARGET PER HOUR). THE CROSS SECTIONS ARE OBTAINED AS THE RATIO BETWEEN THE SEL RATE AND THE HEH FLUX, FURTHER DIVIDED BY 8 (AS EACH BOARD CONTAINED EIGHT CHIPS)

SRAM memory	Beam energy [MeV]	FLUKA HEH flux [cm^{-2}/h]	Measured SEL rate [h^{-1}]	Measured σ_{SEL} per chip [cm^2]
Lyontek	180-210	$1.5 \cdot 10^8$	13.3	$1.1 \cdot 10^{-8}$
ISSI	180-210	$1.6 \cdot 10^8$	6.8	$[3.8 \cdot 10^{-9}, 7.6 \cdot 10^{-9}]$
Samsung	145-195	$1.6 \cdot 10^8$	0	$< 4.4 \cdot 10^{-10}$
Alliance	145-195	$1.5 \cdot 10^8$	0	$< 3.4 \cdot 10^{-10}$

are lower by approximately a factor of 4 compared with the results obtained with a 200-MeV proton irradiation at PSI (see Table II) likely due to a different SEL response to hadrons of different energies, even above the 20-MeV threshold. For the case of the Samsung and Alliance SRAMs, in the absence of observed counts, we place upper limits on the cross sections, that are not inconsistent with the PSI measurements.

V. CONCLUSION

We investigated a test setup where a high-intensity electron beam impacts on an Al-based target with an energy of approximately 200 MeV, or slightly lower. The resulting radiation shower yields a mixed radiation field that includes a relevant neutron flux peaked at the MeV scale, offering interesting prospects for exploitation in the field of R2E.

The setup was studied at the CLEAR accelerator at CERN, normalizing the results to a high-intensity beam operation yielding $6.75 \cdot 10^{15}$ electrons on target per hour. The non-trivial time structure of the CLEAR beam did not affect the experimental results, for which the cumulative rate of electrons on target was the only relevant normalization parameter. From a practical point of view, the CLEAR accelerator was particularly convenient due to its accessibility, as it is detached from the LHC accelerator chain, unlike other CERN facilities, such as CERN high-energy accelerator mixed field/facility (CHARM) [22], [23]. In general, a similar installation can be reproduced at other electron accelerators, provided that they are able to reach similar beam energies and a sufficiently high intensity.

Under the conditions described above, we measured TID rates up to around 300 kGy/h downstream of the target and HEH-eq fluxes up to nearly 10^{10} cm^{-2}/h on the target side, where the TID is sufficiently low to operate electronics for SEU and SEL measurements (e.g., SRAMs). The measured SEU rates were found to be above 10^3 counts per hour with different SRAMs and even close to 10^4 in the case of a Cypress-65 nm. The SEL rates were, instead, significantly lower (and even null in the case of the Samsung and Alliance SRAMs) due to the limited flux of neutrons above 20 MeV in the radiation field. By examining different configurations of the setup, we proved that the TID rate can be suppressed with transverse shielding elements with a low impact on the HEH-eq flux, achieving optimal conditions for SEE testing.

The study in this article was aimed at confirming the viability of an experimental setup yielding neutron-induced SEE measurements at an electron accelerator, especially for the case of SEUs. While this preliminary step was successful, it is clear that some follow-up studies would be needed prior to validating the setup (or a similar one) for SEE testing of electronic components. The accuracy of the neutron energy spectra simulated with FLUKA was indirectly confirmed by the agreement between measurements and predictions that we observed with SRAMs with a different response to intermediate-energy neutrons, but it could be further tested with different experimental techniques to measure the neutron flux. A full overview of the available options is beyond the scope of this work, but an interesting path to follow can be the exploitation of neutron time-of-flight techniques (if allowed by the time structure of the accelerator), as it is done for example at the n_TOF facility at CERN [24]. Moreover, while the setup presented in this article was deliberately very basic, as it was aimed at providing a proof of concept, there is definitely room for further optimization of the size and the material of the target, as well as of the amount of lateral shielding. Such optimization could result in non-negligible variations of the neutron energy spectrum and flux with respect to those presented in this article, as well as of the amount of TID background. A few selected options could be further probed experimentally, and the associated neutron spectra shall be compared in detail with the ones available at other facilities (e.g., neutron spallation facilities [25] or radioactive sources [26]) and with known spectra, such as the atmospheric and ground level ones. Still, even with these changes, the resulting setup would retain the general features highlighted in this document, providing a high flux of neutrons peaked at the MeV scale with a high-energy tail driven by the energy of the primary electron beam, a time structure determined by the electron accelerator, and a level of TID background that depends on the amount of lateral shielding being used.

REFERENCES

[1] M. Brugger et al. (2016). *The CLEAR Facility at CERN*. Accessed: Jan. 5, 2022. [Online]. Available: https://cds.cern.ch/record/2311397

[2] M. Tali et al., "High-energy electron-induced SEUs and Jovian environment impact," *IEEE Trans. Nucl. Sci.*, vol. 64, no. 8, pp. 2016–2022, Aug. 2017.

[3] M. Tali et al., "Mechanisms of electron-induced single-event latchup," *IEEE Trans. Nucl. Sci.*, vol. 66, no. 1, pp. 437–443, Jan. 2019.

[4] D. D. Söderström et al., "Electron-induced upsets and stuck bits in SDRAMs in the Jovian environment," *IEEE Trans. Nucl. Sci.*, vol. 68, no. 5, pp. 716–723, May 2021.

[5] G. Lerner et al., "Analysis of the photoneutron field near the THz dump of the CLEAR accelerator at CERN with SEU measurements and simulations," *IEEE Trans. Nucl. Sci.*, vol. 69, no. 7, pp. 1541–1548, Jul. 2022.

[6] A. Coronetti et al., "SEU characterization of commercial and custom-designed SRAMs based on 90 nm technology and below," in *Proc. IEEE Radiat. Effects Data Workshop*, Santa Fe, NM, USA, Nov. 2020, pp. 56–63.

[7] H. Vincke et al., "Response of alanine and radio-photoluminescence dosemeters to mixed high-energy radiation fields," *Radiat. Protection Dosimetry*, vol. 125, nos. 1–4, pp. 340–344, Mar. 2007.

[8] D. Pramberger, Y. Q. Aguiar, J. Trummer, and H. Vincke, "Characterization of Radio-Photo-Luminescence (RPL) dosimeters as radiation monitors in the CERN accelerator complex," *IEEE Trans. Nucl. Sci.*, vol. 69, no. 7, pp. 1618–1624, Jul. 2022.

[9] M. Cecchetto, R. G. Alía, S. Gerardin, M. Brugger, A. Infantino, and S. Danzeca, "Impact of thermal and intermediate energy neutrons on SRAM SEE rates in the LHC accelerator," *IEEE Trans. Nucl. Sci.*, vol. 65, no. 8, pp. 1800–1806, Aug. 2018.

[10] R. G. Alía et al., "SEL hardness assurance in a mixed radiation field," *IEEE Trans. Nucl. Sci.*, vol. 62, no. 6, pp. 2555–2562, Dec. 2015.

[11] M. Cecchetto et al., "SEE flux and spectral hardness calibration of neutron spallation and mixed-field facilities," *IEEE Trans. Nucl. Sci.*, vol. 66, no. 7, pp. 1532–1540, Jul. 2019.

[12] A. Fassò, "Photonuclear reactions in FLUKA: Cross sections and interaction models," in *Proc. AIP Conf.*, Santa Fe, NM, USA, 2005, pp. 1303–1306.

[13] (Jan. 5, 2022). *FLUKA website*. [Online]. Available: https://fluka.cern

[14] G. Battistoni et al., "Overview of the FLUKA code," *Ann. Nucl. Energy*, vol. 82, pp. 10–18, Aug. 2015.

[15] C. Ahdida et al., "New capabilities of the FLUKA multi-purpose code," *Frontiers Phys.*, vol. 9, Jan. 2022, Art. no. 788253.

[16] K. Roeed et al., "Method for measuring mixed field radiation levels relevant for SEEs at the LHC," *IEEE Trans. Nucl. Sci.*, vol. 59, no. 4, pp. 1040–1047, Aug. 2012.

[17] M. Cecchetto, "Experimental and simulation study of neutron-induced single event effects in accelerator environment and implications on qualification approach," Ph.D. dissertation, Inst. Electron. Syst., Univ. Montpellier, France, 2021. [Online]. Available: https://cds.cern.ch/record/2809556

[18] M. Cecchetto et al., "0.1–10 MeV neutron soft error rate in accelerator and atmospheric environments," *IEEE Trans. Nucl. Sci.*, vol. 68, no. 5, pp. 873–883, May 2021.

[19] M. Cecchetto et al., "Thermal neutron-induced SEUs in the LHC accelerator environment," *IEEE Trans. Nucl. Sci.*, vol. 67, no. 7, pp. 1412–1420, Jul. 2020.

[20] T. M. Flanders et al., "1-MeV equivalent Silicon damage studies at the White Sands Missile Range fast burst reactor," in *Proc. Reactor Dosimetry, 16th Int. Symp.*, M. H. Sparks Eds. West Conshohocken, PA, USA: ASTM International, Dec. 2018, pp. 74–84.

[21] K. Sjobak et al., "Status of the CLEAR electron beam user facility at CERN," in *Proc. IPAC*, 2022, pp. 1–4. [Online]. Available: https://cds.cern.ch/record/2695092

[22] J. Mekki, M. Brugger, R. G. Alia, A. Thornton, N. C. Dos Santos Mota, and S. Danzeca, "CHARM: A mixed field facility at CERN for radiation tests in ground, atmospheric, space and accelerator representative environments," *IEEE Trans. Nucl. Sci.*, vol. 63, no. 4, pp. 2106–2114, Aug. 2016.

[23] D. Prelipcean et al., "Benchmark between measured and simulated radiation level data at the mixed-field CHARM facility at CERN," *IEEE Trans. Nucl. Sci.*, vol. 69, no. 7, pp. 1557–1564, Jul. 2022.

[24] C. Borcea et al., "Results from the commissioning of the n-TOF spallation neutron source at CERN," *Nucl. Instrum. Meth. A*, vol. 513, no. 3, pp. 524–537, Nov. 2003.

[25] C. Cazzaniga and C. D. Frost, "Progress of the scientific commissioning of a fast neutron beamline for Chip Irradiation," *J. Phys., Conf.*, vol. 1021, May 2018, Art. no. 012037.

[26] I. Murata et al., "Neutron and gamma-ray source-term characterization of AmBe sources in Osaka University," *Prog. Nucl. Sci. Technol.*, vol. 4, pp. 345–348, Jan. 2014.